1092
doi: 10.1017/S1431927609093210

Microsc Microanal 15(Suppl 2), 2009
Copyright 2009 Microscopy Society of America

Near / Sub-50 pm TEM Resolution Images of Atoms Simulated with the Second Derivative of the Exit-plane Wavefunction

Hwang Su Kim

Department of Physics, Kyungsung University, Namku, Busan 608-736, South Korea

O'Keefe et al. [1, 2] recently noted the significance of that the second derivative of atom potential forms narrower atom peak with the width only 65 % of the original potential. For zero C_s the image intensity is given by $I(\mathbf{x}) \approx 1 - c\nabla^2 V_p(\mathbf{x})$ under the projected charge density (PCD) conditions [1]. Here $V_p(\mathbf{x})$ is the projected crystal potential on the **x**-plane and $c=\sigma\cdot t\cdot\lambda\cdot\delta f/2\pi$ (σ: the scattering cross-section, t: specimen thickness, λ: electron wavelength, δf: microscope defocus). Due to the second derivative term, $\nabla^2 V_p(\mathbf{x})$, the image of $I(\mathbf{x})$ (PCD form) would show atoms resolved at finer separation with even sub-50 pm. However our calculations showed rather the $\delta f=0$ image gives better resolution in the most realistic cases. To understand this aspect and to search a possible way to obtain a sub-50 pm resolution image, we need first to examine the nature of the exit-plane wave in detail as follows. The **g**-diffracted beam amplitude on the exit plane of a crystal object is,

$$\begin{aligned}\phi_g &= \sum_j C_0^{*(j)} C_g^{(j)} \exp(2\pi i \gamma^{(j)} t) \\ &= \sum_j C_0^{*(j)} C_g^{(j)} [(1 - (2\pi\gamma^{(j)} t)^2/2 + \text{higher terms}) + i(2\pi\gamma^{(j)} t - \text{higher terms})] \qquad (1)\end{aligned}$$

For the meanings of symbols in (1) and other details, one should refer to [3]. It should be noted that $\sum_j C_0^{*(j)} C_g^{(j)} = \delta_{g,0}$, $\sum_j \gamma^{(j)} C_0^{*(j)} C_0^{(j)} = 0$ and $2\pi\sum_j \gamma^{(j)} C_0^{*(j)} C_g^{(j)} = \sigma V_g$ for $g \neq 0$ [4]. If t is very small and the higher terms including the square term in (1) are ignored, then the inverse Fourier transform of ϕ_g gives the exit-plane wavefunction for a weak phase object, $\Psi(\mathbf{x}) \approx 1 + i\sigma\cdot t\cdot V_p(\mathbf{x})$. Under these conditions the PCD form of $I(\mathbf{x})$ can be derived approximately. However for t= 4nm ~10 nm range suitable to HRTEM specimen, the higher terms cannot be simply ignored. Thus the weak phase object approximation and accordingly the PCD form of I(x) are no longer generally valid. In (1) the important Bloch waves are for $\gamma^{(1)} \sim 0$ and $\gamma^{(2)} \sim (-\lambda g^2/2)$. If these two Bloch waves are taken only, (1) becomes the kinematical scattering diffraction amplitude.

And $-\sum_j C_0^{*(j)} C_g^{(j)} (2\pi\gamma^{(j)} t)^2/2 \approx (\pi\lambda\sigma\cdot t^2/2) g^2 V_g$; the inverse Fourier transform of this term plus $\delta_{g,0}$ gives the (real) wave function, $1-(\lambda\sigma\cdot t^2/8\pi)\nabla^2 V_p(\mathbf{x})$. The similar argument can be applied to the higher terms too. Thus we can roughly say that the imaginary part image of the exit-plane wave function will reflects a crystal potential and its real part image will show narrower peaks of the charge density but with weak contrast under the kinematical scattering approximation.

The argument above was carefully checked with test specimens of silicon, InAs & diamond through image simulations. From these simulations we realized that for the case of specimen thickness above 4 nm and 300 Kev electron beam, the exit-plane wavefunction do not give near/sub-50 pm resolution images as can be seen in the 1st rows of Fig. 1 and 2. (Applying the contrast transfer function with a certain δf and $C_s=0$ to the wavefunction usually gives rather deteriorated images in this case). However we found the images from its second derivative of the exit-plane wavefunction indeed give clear near/sub-50 pm resolution images, as shown in the 2nd rows in Fig.1 and 2. This resolution improvement, in fact, comes from that if a peak shape is like a Gaussian distribution function, its second derivative becomes a narrower peak function with the reduced width.

https://doi.org/10.1017/S1431927609093210 Published online by Cambridge University Press

In summary, obtaining near/sub-50 pm resolution images shown in figures in experiment requires the exit-surface plane wavefunction for the information limit beyond 50 pm, which may be retrieved from a focal series reconstruction using a high stable 300 Kv TEM (in this case) and the procedure of the second derivative of the wavefunction.

References

[1] M.A. O'Keefe, L.A. Allard & D.A. Blom, Microsc. Microanal. **13** (2007) 872-873.
[2] M.A. O'Keefe, Ultramicroscopy **108** (2008) 196-209.
[3] P.B. Hirsch, A. Howie, R.H. Nicholson, D.W. Pashley, and M.J. Whelan, *Electron Microscopy of Thin Crystals*, Krieger Publ., Huntington (N.Y.) 1977.
[4] H.S. Kim and S.S. Sheinin, Ultramicroscopy **51** (1993) 109-116.

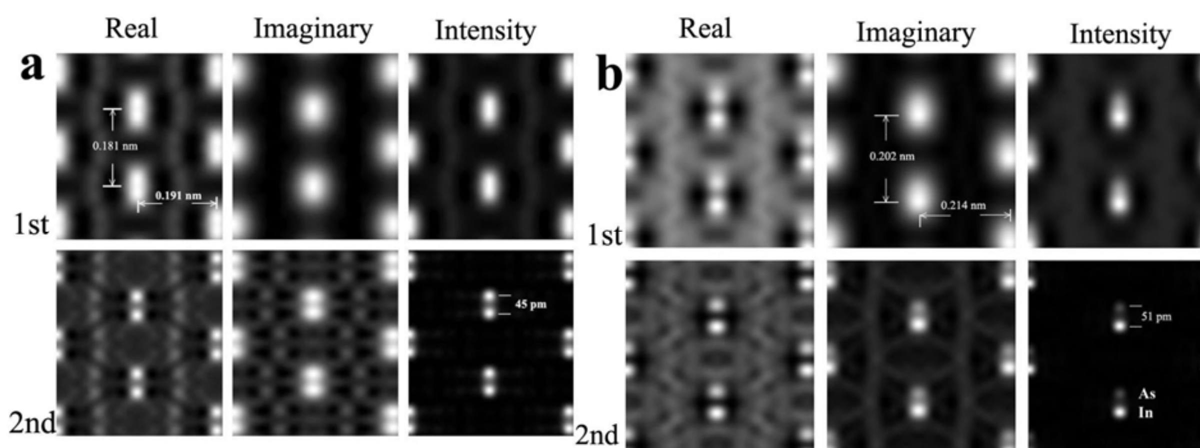

Fig. 1. a: for silicon (0.543 nm DC), b: for InAs (0.606 nm DC) with t=4nm in [114] orientation. The images in the 1st row are for the real part, the imaginary part and the intensity of the exit-plane wave function. The 2nd row images are for the negative of the second derivative of the real and the imaginary functions, and its absolute square intensity. Debye-Waller factors at room temperature, 0.467 $Å^2$ of Si(a) and 0.5 $Å^2$ of InAs(b), were given in calculations. The contrasts of all images were adjusted as 1 to see clear images.

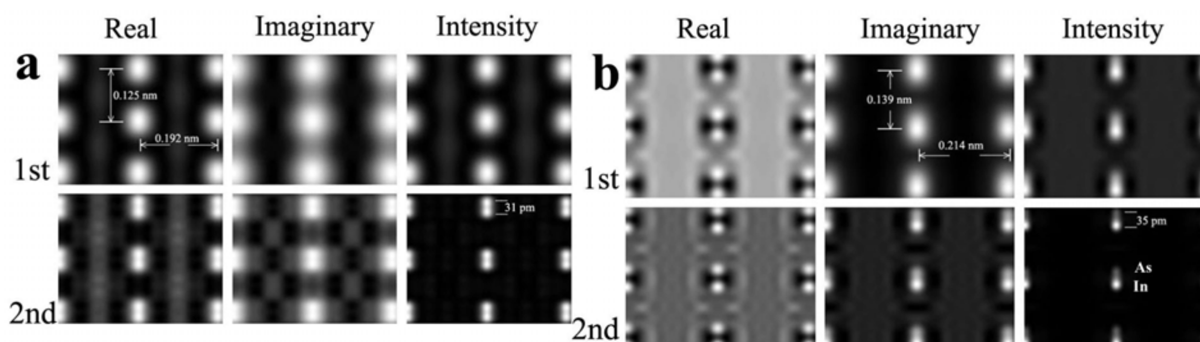

Fig. 2. The same as those in Fig. 1 but for [116] orientation.

https://doi.org/10.1017/S1431927609093210 Published online by Cambridge University Press